13th Int Symp on Applications of Laser Techniques to Fluid Mechanics
Lisbon, Portugal, 26-29 June, 2006
Paper: 1019

Supersonic Flow Field Investigations Using a Fiber-optic based Doppler Global Velocimeter

James F. Meyers[1], Joseph W. Lee[2], Mark T. Fletcher[2], Angelo A. Cavone[3], and J. Ascención Guerrero Viramontes[4]

1: Distinguished Research Associate of NASA Langley Research Center, Hampton, Virginia 23681, United States james.f.meyers@larc.nasa.gov
2: NASA Langley Research Center, Hampton, Virginia 23681, United States
joseph.w.lee@nasa.gov, mark.t.fletcher@nasa.gov
3: Swales Aerospace, NASA Langley Research Center, Hampton, Virginia 23681, United States
A.A.Cavone@larc.nasa.gov
4: Old Dominion University, Norfolk, Virginia 23502, United States
(currently: Centro de Investigaciones en Optica A.C., Leon, México)

Abstract A three-component fiber-optic based Doppler Global Velocimeter was constructed, evaluated and used to measure shock structures about a low-sonic boom model in a Mach 2 flow. The system was designed to have maximum flexibility in its ability to measure flows with restricted optical access and in various facilities. System layout is described along with techniques developed for production supersonic testing. System evaluation in the Unitary Plan Wind Tunnel showed a common acceptance angle of f4 among the three views with velocity measurement resolutions comparable with free-space systems. Flow field measurements of shock structures above a flat plate with an attached ellipsoid-cylinder store and a low-sonic boom model are presented to demonstrate the capabilities of the system during production testing.

1. Introduction

In the sixteen years since Komine (1990) invented Doppler Global Velocimetry (DGV), it has been relatively slow in acceptance because its advantages did not compensate for its complexities when compared with Particle Image Velocimetry (PIV). Its ability to make three-component velocity measurements from very small particles (<0.1 micron) was the greatest advantage. However, its lack of velocity measurement resolution (~2 m/s) gave PIV the edge in acceptance. Then Nobes *et al* (2002) at Cranfield University developed a DGV system that used a fiber optic bundle to view the laser light sheet. This specially constructed bundle consisted of four individual bundles woven together to present the three component images and the laser beam to a single receiver system. Instantly the cost of a three component DGV system was reduced significantly, and the potential opened for measuring velocity images in areas with restricted access – a capability that is not possible with PIV. Quick to adopt this major advance, Willert *et al* (2003) obtained a duplicate fiber optic bundle and designed a hardened DGV system around it. This work led to the first ever non-intrusive planar velocity measurements of a cryogenic wind tunnel flow field. The flow was seeded with steam injection, which produced very small ice particles that provided sufficient scattered light to clearly delineate the vortical flow field under investigation. The hostile environment, limited optical access, and long focal distances required elevates the significance of this accomplishment. No other currently available technique was capable of making these measurements.

As with any major breakthrough however, the research showed a few shortcomings, notably problems with the custom fiber bundle. The desire to obtain good optical quality resulted in a large fiber bundle that was very fragile resulting in many broken fibers. These produced black holes within the image, (Nobes *et al* (2002), Willert *et al* (2003)). Additionally the careful alignment of the individual fibers in parallel rows to yield the best image quality resulted in a rectangular grid

overlaying the image. Unfortunately, it is not possible to remove the grid formed by the holes between the fibers with image processing techniques without compromising the data.

Beyond the advantages outlined above, interest at NASA Langley Research Center in the use of fiber bundles was as a potential solution to the development of a practical three-component DGV system for the Langley Unitary Plan Wind Tunnel (UPWT). An attempt to construct a three-component DGV system using free-space optics resulted in the complicated system shown in Figure 1. While this system measured the supersonic flow field, the image area was fairly small and the system could not be translated. Using fiber bundles, the resulting system, Figure 2, was greatly reduced in complexity, and increased the available measurement area while affording greater flexibility in measurement location. These characteristics along with the ability of the model sting to translate 900 mm in the axial direction resulted in a very flexible measurement system to investigate supersonic flows. Following are descriptions of the system characteristics, results of performance testing to characterize the system, and the investigation of shock wave structures generated by a low-boom model at Mach 2.

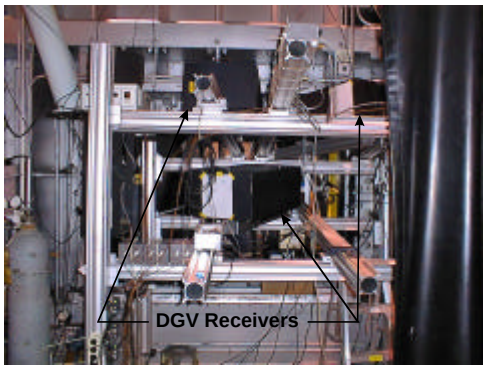

Figure 1. – Free-space, three-component Doppler Global Velocimeter installed in the UPWT.

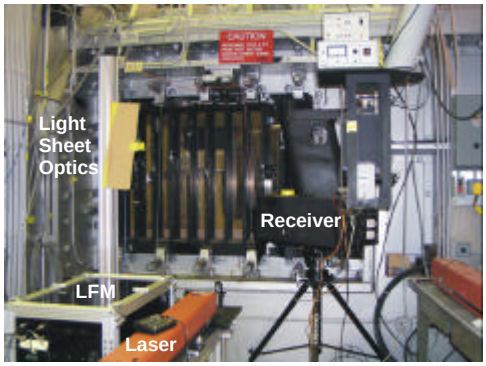

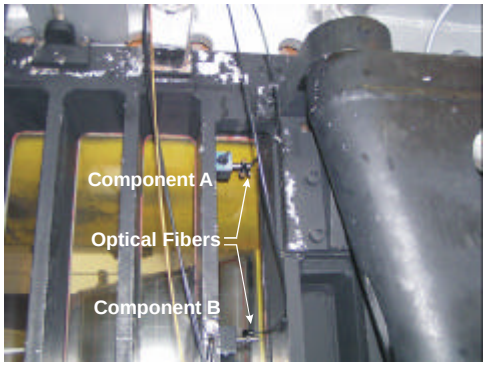

Doppler Global Velocimeter

Fiber-optic viewing system

Figure 2. – Fiber-optic based, three-component Doppler Global Velocimeter installed in the UPWT.

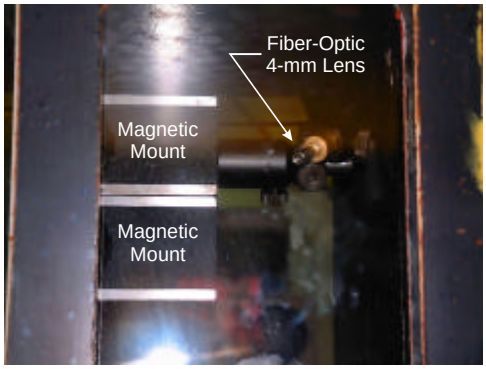

Figure 3. – 4-mm diameter collecting lens attached to the optical fiber bundle installed in the UPWT.

2. Optical Fiber-Bundle Based Doppler Global Velocimeter

The development of an optical fiber-bundle based Doppler Global Velocimeter at NASA Langley deviated from the work of Nobes *et al* (2002) and Willert *et al* (2003) in that fiber flexibility was a primary concern, even if image quality would be slightly compromised. Flexibility was important because of restricted optical access in several Langley wind tunnels along with a desire to potentially place the fibers inside large wind tunnel models. Three separate fiber bundles were desirable since they afforded the ability to customize the arrangement of the DGV system to accommodate a given facility/test configuration. A search for the smallest diameter, highest image quality fiber resulted in the selection of a fiber bundle offered by Myriad Fiber Imaging Technology. This fiber bundle was 1.0 mm in diameter and contained 50,000 individual fibers sheathed within a plastic outer covering resulting in an overall diameter of 3.0 mm. The distal end of the 3.0-m long fiber had a

changeable collecting lens system with a 4.0 mm collecting aperture, Figure 3. The proximal end was sheathed in a stainless steel tube with a wall thickness of 0.1 mm. This allowed the three fiber bundles to be placed close together in the imaging plane of the DGV receiver. This allowed maximum magnification of the three fiber images, Figure 4. Finally, the Laser Frequency Monitor (LFM) was constructed by transmitting a portion of the laser beam to the viewing plane of the DGV receiver via a 400-micron multimode optical fiber.

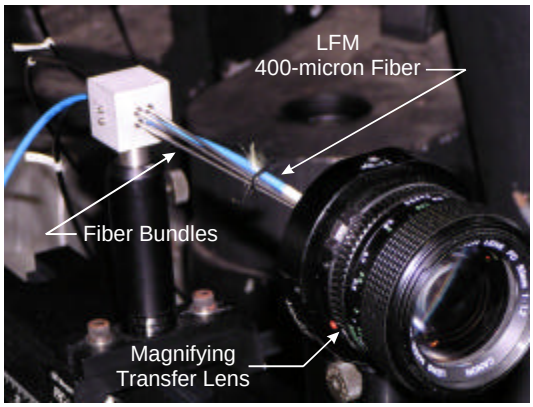

Figure 4. – Fiber optic proximal ends and transfer lens for three-component DGV system.

Once construction was completed, laboratory testing was conducted to evaluate image quality and system performance. A spatial calibration target, consisting of a rectangular grid of black dots on a white background with 25.4-mm spacing, was used to investigate image quality. The camera image of the target viewed through the three fibers is shown in Figure 5(a). An image-enhanced magnified portion of one of the fiber bundles to accentuate the patterns of the individual fibers is shown in Figure 5(b). The dense packing of the fibers results in very minor edge effects that are easily removed with two applications of a 3x3-pixel median filter. The expected low-pass characteristics, as visualized by the blurry dots in Figure 5, are the result of the low modulation transfer function (MTF) of the 4.0-mm lens imaging the target onto the 1.0-mm diameter fiber bundle. Dewarping this image using bi-linear techniques (Meyers (1992)) yields a 229-mm square common area among the three views, Figure 6, at a focal distance of 1.0 m (f4.4). The imaging system modulation transfer function was consistent among all three-fiber bundles, and caused a blurring of the sharp dot edges by 25 pixels in the dewarped image. Therefore sharp discontinuities in the flow velocity caused by shocks would also be blurred by 25 pixels, or 5.6 mm for this field of view.

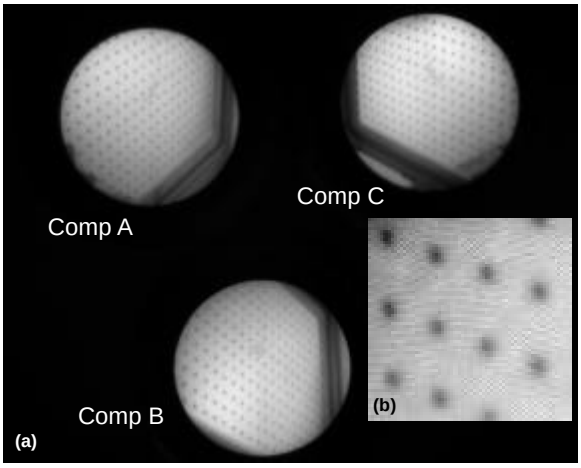

Figure 5. – Camera image of the spatial calibration target viewed by the three fiber bundles.

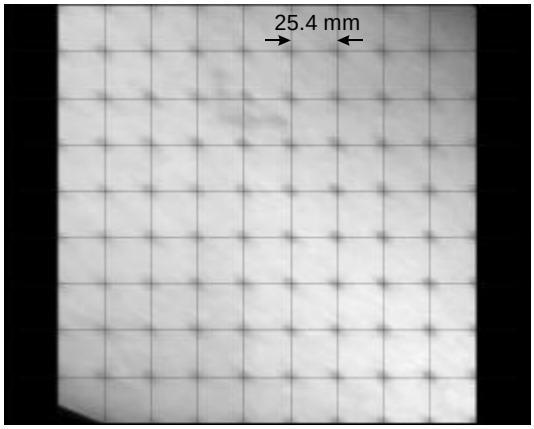

Figure 6. – Grid overlaid dewarped spatial calibration target.

As expected the collected light levels obtained with the 4.0-mm viewing lens are significantly lower than a typical free-space system. Increasing the integration time on the 12-bit electronically cooled 1280x1024-pixel CCD cameras to 1.2 seconds resulted in acceptable signal levels.

3. System Evaluation in a Supersonic Wind Tunnel

A simulated Space Shuttle model was constructed using an ellipsoid-cylinder store attached to a flat plate, Figure 7. This model would produce shock structures that would be representative of

those produced by the Shuttle Solid Rocket Booster (SRB) as they impact the External Tank. Placing the store 190-mm downstream of the flat plate leading edge provided the opportunity to also investigate the system response to a simple oblique shock. Inclining the flat plate to -3.0 degrees produced an oblique shock attached to the plate leading edge. This shock would have a clear delineation with uniform velocities above and below the shock. Temporal and spatial statistics obtained within the uniform velocity area would provide measurement noise levels. Moving the model upstream would bring the conical shock from the ellipsoid-cylinder store within the measurement area. This would determine if the system were capable of measuring the shock structure and any reflection from the flat plate. Finally, a 400-micron multimode optical fiber was embedded in the flat plate oriented to launch a laser beam orthogonal to the model surface. The particle-scattered light from the beam would be viewed by the fiber-optic system in an attempt to measure the boundary layer velocity profile. Bringing the laser beam from inside the model would eliminate surface scatter generated by external laser illumination passing/striking the model.

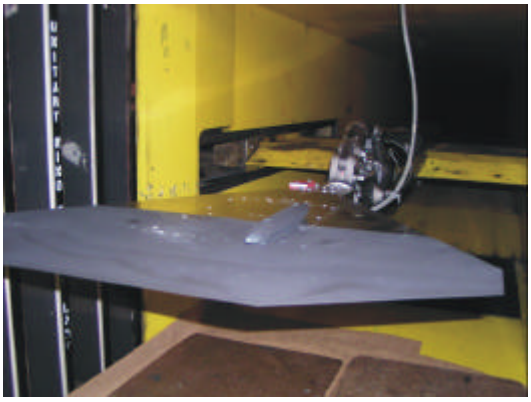

Figure 7. – Flat plate model with attached ellipsoid-cylinder store installed in the UPWT.

3.1 Experimental Setup

The fiber-optic based DGV system was installed in the Unitary Plan Wind Tunnel, Figure 2. Two fibers were located at the top corners of the door and the third fiber located on the upstream side just above the tunnel centerline to view the flow above the flat plate model. This configuration yields good velocity measurement resolution U (streamwise) and V (crossflow), but poorer W (vertical) resolution. The laser light sheet was produced using a cylindrical lens and orientated vertically passing through the center door window in the crossflow direction. A standard small frame Argon ion laser was frequency stabilized by locking it to a selected location along an iodine transition. The frequency stabilization was based on a feedback control system that compensates for any thermal-induced changes that occur in the laser resonator (Förster *et al* (2000), Lee and Meyers (2005)). The resulting system had a random variation in optical frequency with a maximum drift of less than 1.0 MHz/min within the limits of ±5.0 MHz over a 90-minute acquisition period. The iodine vapor cell was vapor limited at 40^{o} C and operated at 60^{o} C (Elliot *et al* (1994), Forkey (1996)). An overlapping piecewise optical frequency calibration was performed using a variable frequency Bragg cell in 10 MHz steps over a 240 MHz range for each laser longitudinal mode throughout the iodine absorption line (Lee and Meyers (2005)).

Normally DGV systems are operated with the laser frequency adjusted to the midpoint along the side of the absorption line. The large Doppler frequencies that were expected at Mach 2 with the optical geometry set for maximum three-component accuracies prohibit this approach. Instead the laser frequency was tuned to the bottom of the absorption line. The Doppler shifts from the two components with the collecting optics upstream would result in scattered light frequencies that would lie along the left side of the absorption line. Doppler shifts from the third component would result in scattered light frequencies that would lie along the right side of the absorption line. Since the laser frequency could not be determined at the bottom of the absorption line, a dual-pass Bragg cell (Lee and Meyers (2005)) was used to shift the LFM optical frequency (and laser stabilization beam frequency) to the midpoint along the left side of the absorption line. These frequency locations are shown positioned along the iodine vapor cell calibration profile in Figure 8.

The optical system was orientated to view a square area, 229 mm on a side, in the crossflow plane. The area was centered in the crossflow direction and set vertically to extend about 25 mm below the top of the flat plate. The leading edge of the model was translated from 25 mm downstream of the light sheet to 394 mm upstream. This provided two flow fields: an oblique shock from a classic sharp leading edged flat plate, and a conical shock from the store interacting with a flat surface in close proximity.

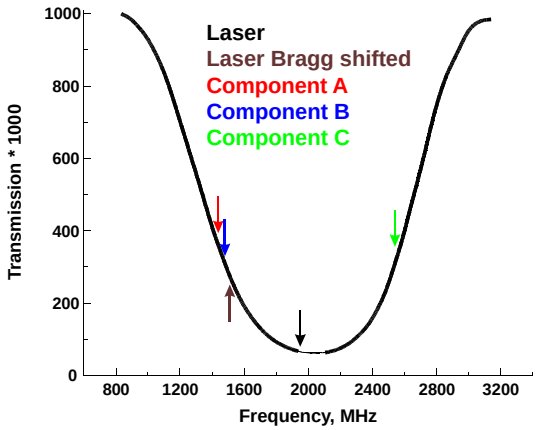

Figure 8. – Iodine calibration profile with laser, Bragg-shifted laser, and Doppler shifted component frequencies located at Mach 2 (freestream = 520 m/s).

The Langley Unitary Plan Wind Tunnel is a closed circuit, continuous-flow, variable-density supersonic wind tunnel. Test section 1 has a 1.22-x 1.22-m cross section and a variable flow Mach number from 1.5 to 2.9. The tunnel was operated at Mach 2 and the flow seeded with water condensation. Approximately 3 liters of water was injected at the beginning of a test run which provided seeding throughout the 90-minute test time. Condensation particles were estimated to be less than 0.15-micron in diameter (Shirinzadeh *et al* (1991)).

A typical acquisition of velocity data began by setting the model at the desired streamwise location. After insuring that the laser was operating at the selected single frequency and the laser stabilization system locked to that frequency, the automated data acquisition/processing was started. The data acquisition computer set the camera integration time to 1.2 seconds and began the acquisition of 50 image pairs. Once acquired, the data images were transferred to the data acquisition and data processing computers to provide redundant data storage. The data processing parameter file was constructed on the data acquisition computer based on system and flow characteristics and user selected parameters. Once completed, the data processing parameter file was transferred to the data processing computer, and that computer automatically began to process the acquired data set and subsequently display the resulting orthogonal three-component velocity data. The total data acquisition time was approximately two minutes, one minute to acquire the images and ten seconds to transfer the data to the computers. The remaining 50 seconds was needed to move the model to the next location. Total data processing time was approximately 25 seconds plus a result display time of 20 seconds. The data acquisition computer returned to user control following transmission of the data processing trigger.

3.2 Data Processing Procedures

Data processing consisted of a series of image processing steps applied to the data images to develop the orthogonal three-component velocity flow field maps of the shock structures above the model (Meyers (2005)). The signal and reference data images were averaged respectively to increase signal-to-noise ratio. Background images, obtained with full system and tunnel operation prior to the injection of seeding, were then subtracted to remove extraneous laser and test section light contributions. The LFM portion of the two average images were segregated and spatially integrated. The integrated signal value was normalized by the integrated reference value to yield the ratio that was proportional to the optical frequency of the laser. The ratio was multiplied by a scaling factor to match the original iodine vapor calibration. The iodine calibration was then interrogated to determine the laser frequency.

These same processing steps were also incorporated in the component image processing. Bi-linear dewarping techniques were used to segregate each component image from the background-removed camera images. In addition perspective and optical distortions were eliminated yielding

identical mapping of the three component images. Each average component image, signal and reference, were spatially filtered using a median filter set to the MTF of the system (25-x25-pixels after dewarping magnification). The resulting images were interrogated to zero any pixels within areas containing high spatial frequency intensity gradients to avoid normalization anomalies. The signal image was then normalized by the reference image on a pixel-by-pixel basis. The resulting ratio image was multiplied by the scaling factor image obtained under freestream conditions with the Doppler-shifted laser frequencies tuned outside the iodine absorption line. In addition, it was assumed that any patterns found in freestream velocity images were due to optical effects not accounted for in the scale factor mapping, e.g., interference fringes, window transmissivity variations, etc. A correction image was developed to negate these effects based on B-spline techniques to yield smooth freestream images. The ratio image was then multiplied by this correction image to yield a ratio image without anomalies. The ratio image was low pass filtered to remove any normalization noise effects. The ratio image levels were translated, pixel-by-pixel, through the iodine vapor calibration to yield the optical frequency map. Subtracting the laser optical frequency obtained from the LFM yields the Doppler frequency map. The component velocity map was then determined based on the optical geometry and the Doppler equation. Finally, the three measured components, A, B, and C were transformed to yield the orthogonal velocity components U, V, and W. User options in the setup file provide pseudo color display of any or all of the calculated images. The final streamwise pseudo color, crossflow vector map, e.g., Figure 9, was always displayed for 20 seconds to serve as a data monitor to allow data quality evaluation.

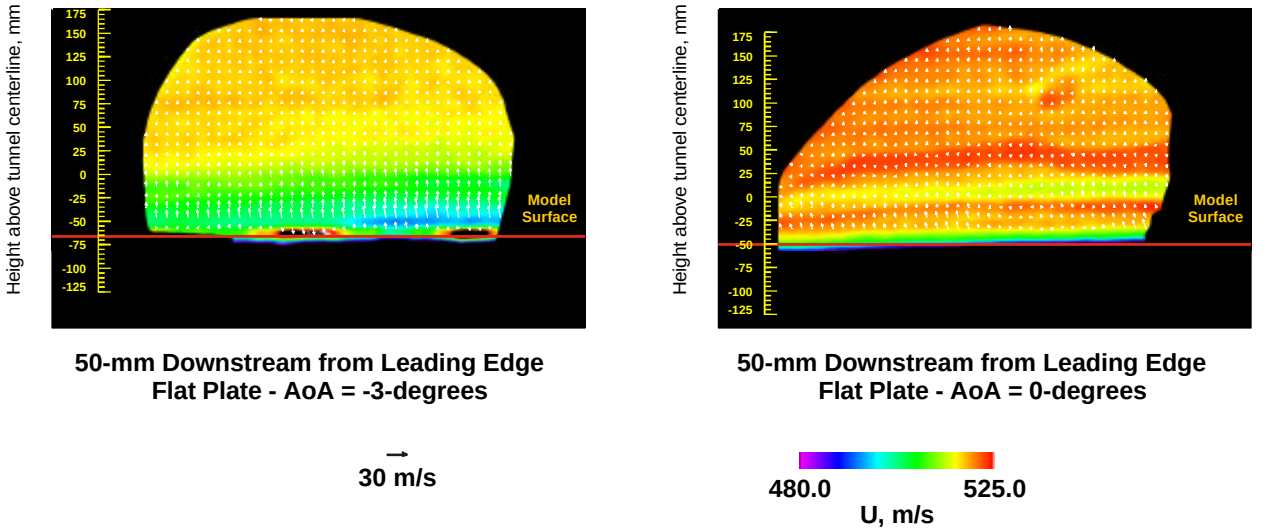

Figure 9. – Three-component velocity measurements of the oblique shock 50-mm downstream of the flat plate leading edge.

3.3 Measurement Evaluation

The resolved U, V, and W velocity maps of the flow field were evaluated with the flat plate set to an inclination angle of –3.0-degrees and the freestream Mach number set to 2.0. The portion of the flow above the oblique shock (freestream) 50-mm downstream of the leading edge, Figure 9, was interrogated spatially and temporally to determine measurement consistency and noise levels. Spatial consistency was determined by calculating the average and standard deviation of the freestream pixel measurements in the average velocity image, Figure 9:

	Spatial average (m/s)	Standard deviation (m/s)
U (freestream)	516.6	0.90
V (crossflow)	-0.5	0.37
W (vertical)	1.8	1.39

Temporal consistency was determined by calculating the average and standard deviation for each corresponding pixel location in the 50 individual velocity image measurements. The total average velocities and average standard deviations were:

	Spatial average (m/s)	Standard deviation (m/s)
U (freestream)	516.6	1.70
V (crossflow)	-0.2	1.28
W (vertical)	3.1	5.18

These results indicate that the fiber-optic based DGV system has measurement uncertainties comparable to free-space systems. If facility optical access is limited, as in the UPWT, compromises made to install a free-space system, Figure 1, would yield measurement uncertainties far worse than found above. These uncertainties would be primarily attributed to spatial view limitations, optical distortions, and geometric coupling errors. Geometric limitations were found in the above statistics because the span in the vertical direction was only 35-percent of the horizontal span resulting in the larger uncertainties in the W-velocity component. The measured streamwise velocity of 516.6 m/s was consistent with tunnel throat block settings and compressor speeds that would yield a velocity in the neighborhood of 520 m/s at Mach 2.

The shock boundary shown in Figure 9 is not razor sharp, but there is little uncertainty as to its location. The crossflow velocity was found to be small and random in direction above the oblique shock, but clearly directed behind/below the shock representing an upward flow angle change of approximately 2.25-degrees. When the flat plate was set to an inclination angle of 0.0-degrees, the drop in the streamwise component velocity occurred only in the immediate vicinity of the shock, Figure 9. These flow characteristics continued downstream as the corresponding measurements 100-mm downstream of the leading edge indicate in Figure 10.

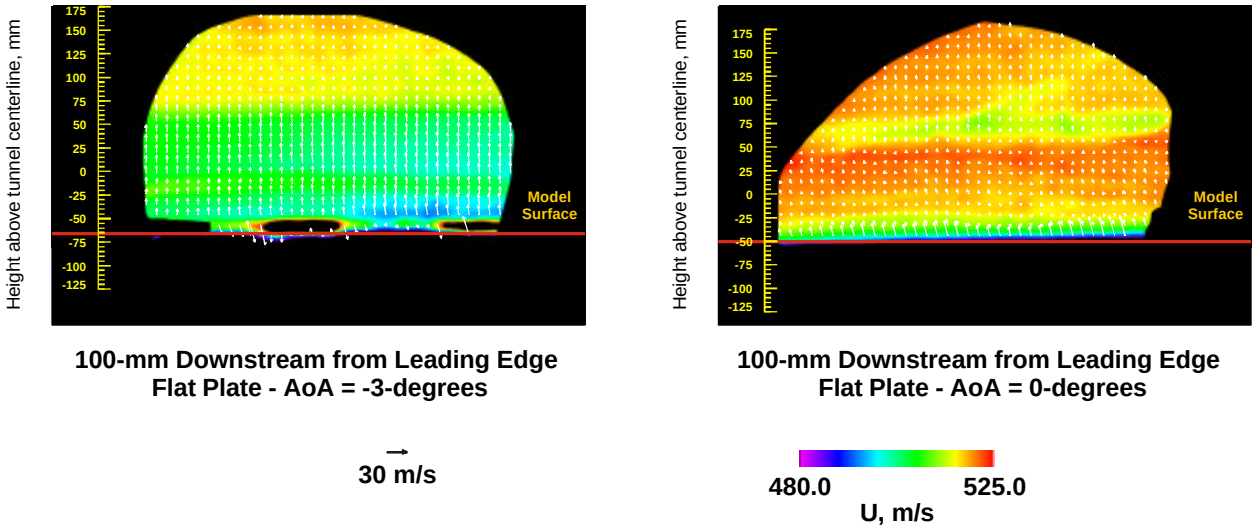

Figure 10. – Three-component velocity measurements of the oblique shock 100-mm downstream of the flat plate leading edge.

Moving the model further upstream brought the conical shock from the ellipsoid-cylinder into the measurement region. The ability of the fiber-optic DGV system to delineate the complicated flow field is illustrated in Figure 11, 100-mm and 137-mm downstream of the nose of the store, respectively. The sudden change in direction of the crossflow velocity is clearly found at the shock location. The mapping of the flow field included 43 measurement planes, 6.4 mm apart in the axial direction requiring approximately 90 minutes of tunnel run time to complete. Thus the ability to perform production testing yielding real-time results of detailed, high-speed flows was demonstrated.

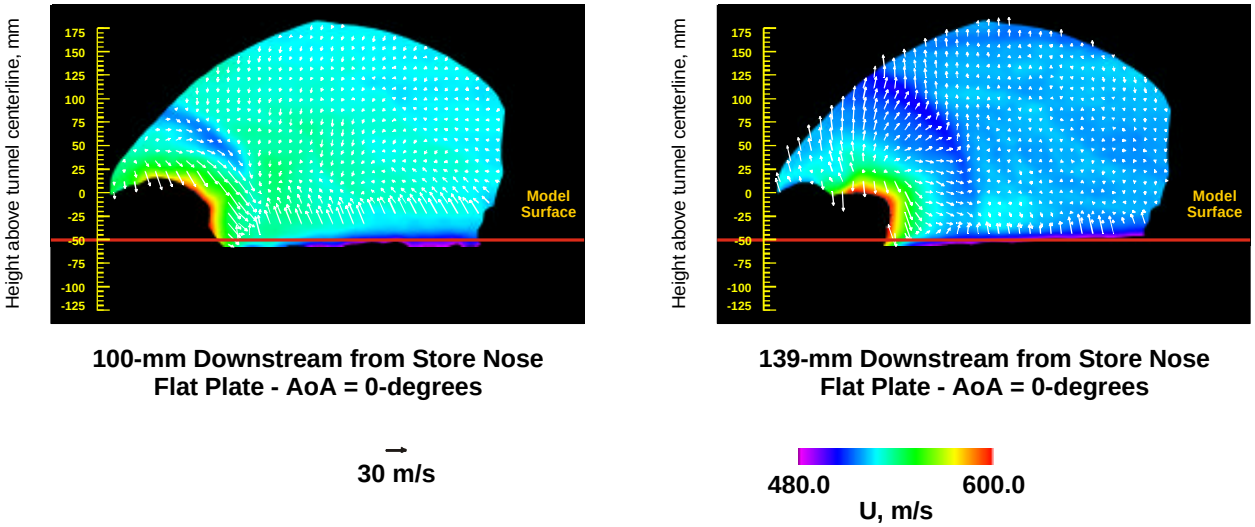

Figure 11. – Three-component velocity measurements of the conical shock generated by the ellipsoid-cylinder store.

The last part of the test series was to redirect the laser beam into the multimode optical fiber embedded in the model to launch a vertical laser beam. The model was moved in the axial direction to place the laser beam in the measurement plane. A normal data acquisition was performed and the data processed along the laser beam. The results indicated that the model had deflected slightly under load angling the beam out-of-plane. Thus conversion of the components A, B, and C to orthogonal components would not be accurate. However, plots of the three component velocity profiles, Figure 12, clearly show measurements of the boundary layer.

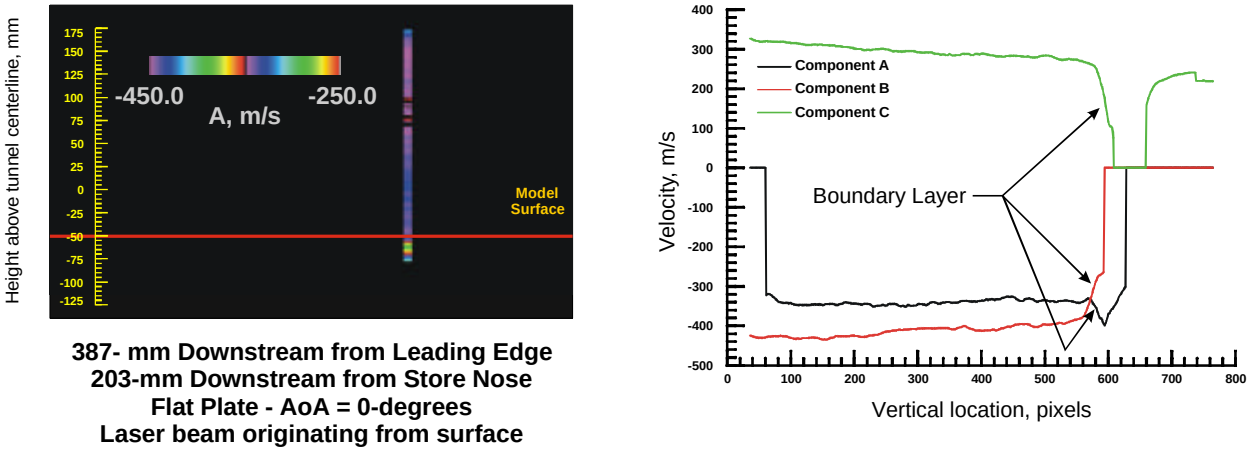

Figure 12. – Three-component velocity measurements of the flow boundary layer using a laser beam emitted from an embedded multimode fiber mounted perpendicular to the flat plate surface.

4. Supersonic Flow Measurements – Low-Boom Model

Although the fiber-optic based DGV system was successful in the production testing demonstration of detailed supersonic flow fields, these capabilities were to be stressed further in a second entry. The objective was to map the shock structures generated by a low-sonic boom model, Figure 13, at the model design Mach number of 2. The expected flow field would contain shock structures far weaker than those obtained from the flat plate model. Additionally, these structures would interact with wing tip vortex structures. The system configuration was altered to move the fiber located at the tunnel centerline to the bottom of the test section window since model blockage was no longer an issue. This expanded the vertical separation to 75-percent of the horizontal span and thereby increasing W-component accuracy. The model was not only translated in the axial direction, but laterally to follow the shock structures further downstream to the maximum of five model spans. The final data set was a combined patchwork of the various data sets obtained for different model locations that were acquired over several days.

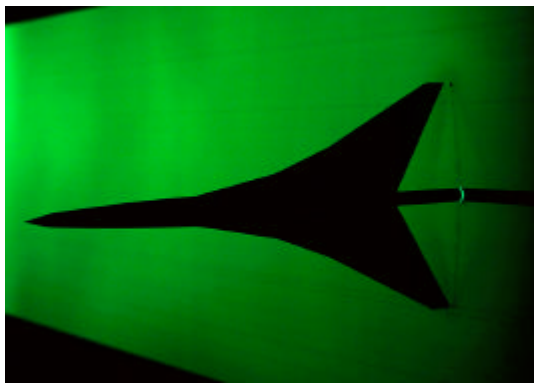

Figure 13. – Low sonic boom model.

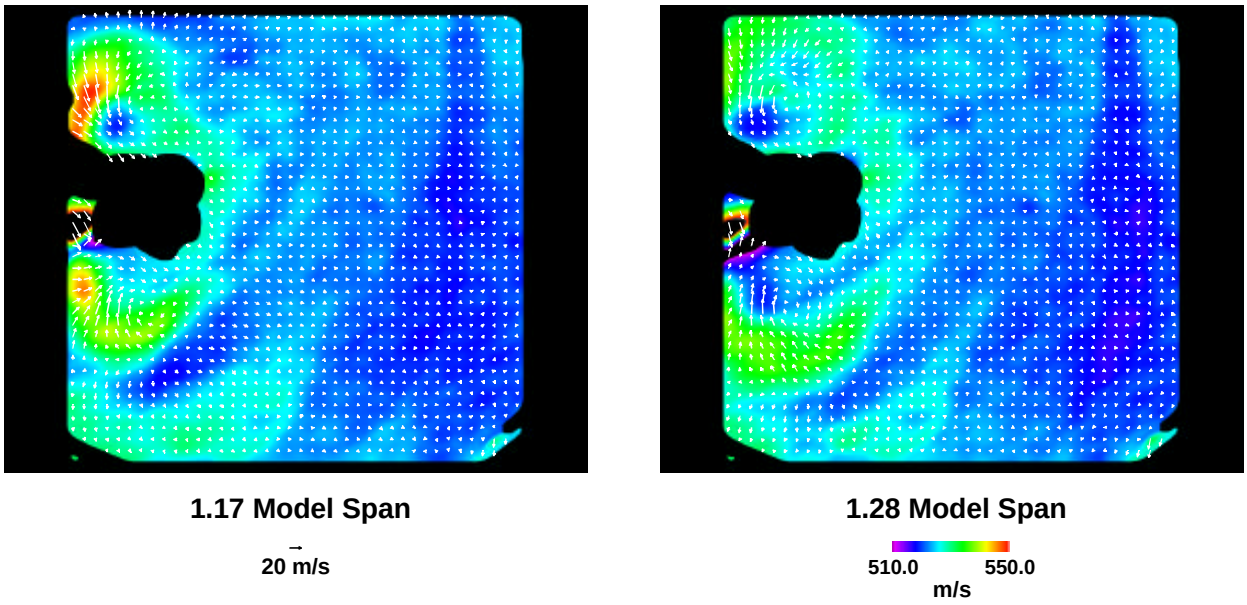

Figure 14. – Three-component velocity measurements of the flow field downstream of the low sonic boom model at Mach 2.

The velocity map obtained at 1.39 model span, Figure 14, illustrates the complicated nature of the flow field. The model is located on the left of the velocity map and rotated counter clockwise 90-degrees making the top of the model toward the left side of the map. The weak bow shock is found on the right of the map and the stronger wing shock left of center. Two high-speed jets are found to the left

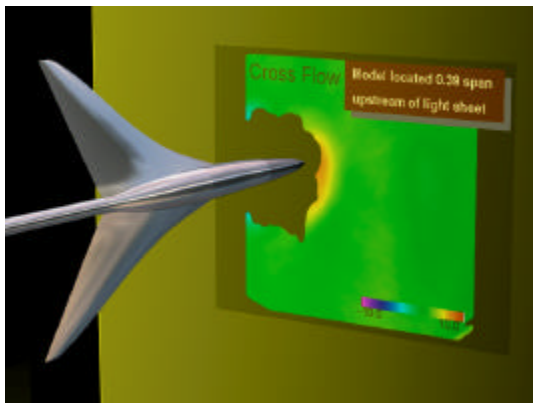

Figure 15. – Crossflow velocity measurements of the flow field about the low sonic boom model at Mach 2 – 0.39 model spans.

of the model (lower left of the map). The closer jet rising from the fuselage area has a matching jet to the right of the model (upper left of the map). The second jet is separating from the wing shock as it rises above the model. The corresponding jet to the right of the model is missing, most likely contaminated by secondary scattering originating from particle scatter reflecting back from the upstream model. The two wing tip vortices are clearly found by viewing the rotating crossflow velocity vectors. Of the individual velocity components, the crossflow velocity (flow toward the ground / right of map) was the most sensitive. Examples of this component measurement are shown in Figures 15-17 for model spans of 0.39, 1.17, and 1.39, respectively. With a full crossflow velocity range extending from –10 m/s to 10 m/s, the shock patterns and vortex locations are easily located. The smoothness and consistency of the velocity contours indicate that the measurement characteristics determined during the flat plate test were maintained in the low-sonic boom investigation. The system sensitivity allowed the tracking of the shocks though the full traverse of five model spans, Figure 18. This mapping of the wing shock at five model spans has a peak-to-peak velocity difference of 4 m/s, down from a difference of 13.8 m/s at 1.39 model spans, as the shock dissipated downstream.

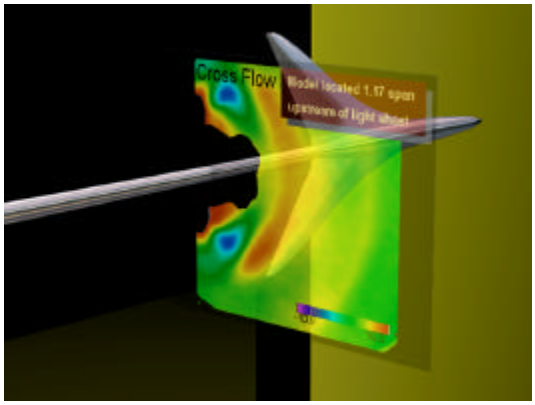

Figure 16. – Crossflow velocity measurements of the flow field about the low sonic boom model at Mach 2 – 1.17 model spans.

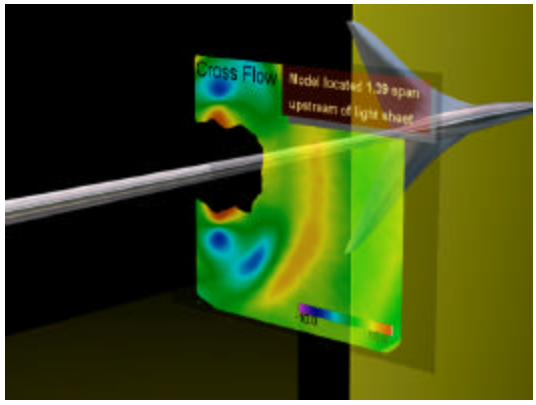

Figure 17. – Crossflow velocity measurements of the flow field about the low sonic boom model at Mach 2 – 1.39 model spans.

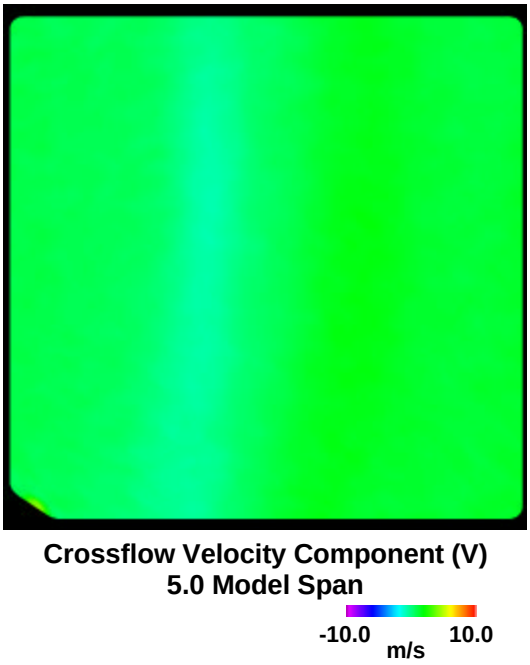

Figure 18. – Crossflow velocity measurements of the flow field about the low sonic boom model at Mach 2 – 5.0 model spans.

5. Summary

A three-component fiber-optic based Doppler Global Velocimeter has been described. Evaluations of its performance have shown measurement resolutions comparable to free-space DGV systems. Although spatial sharpness was less, the ability of the small individual fiber bundles and 4-mm collecting lenses to view flow fields with restricted access provided planar measurements not possible with any other technique. No broken fibers were found in two years of laboratory testing and two wind tunnel entries. Techniques and procedures for production testing in a supersonic wind tunnel were described. Flow field measurements of an oblique shock from a sharp edged flat plate, conical shock from an ellipsoid-cylinder, and shock structures generated from a low-sonic boom model indicate the ability of the system to measure three components of velocity in Mach 2 flows. Additionally, measuring the

boundary layer above a flat plate in a Mach 2 flow using a laser beam exiting the plate from an embedded optical fiber was demonstrated.

6. References

Elliot, G.S.; Samimy, M.; Arnette, S.A. (1994): *Details of a molecular filtered-based velocimetry technique*. 32nd Aerospace Sciences Meeting and Exhibit, Reno, NV, paper no. AIAA-94-0414, January 10-13, 1994.

Forkey, J.N. (1996): *Development and Demonstration of Filtered Rayleigh Scattering – A Laser Based Flow Diagnostic for Planar Measurement of Velocity, Temperature and Pressure.* Princeton University Department of Mechanical and Aerospace Engineering Technical Report 2067, 1996

Förster, W.; Karpinsky, G.; Krain, H.; Röhle, I.; and Schodl, R. (2000): *3-component-Doppler-laser-two-focus velocimetry applied to a transonic centrifugal compressor.* 10th International Symposium on Applications of Laser Techniques to Fluid Mechanics, Paper 7-2, Lisbon, Portugal, July 10-13, 2000.

Komine, H. (1990): *System for Measuring Velocity Field of Fluid Flow Utilizing a Laser Doppler Spectral Image Converter*. U.S. Patent No. 4,919,536, April 24,1990.

Lee, J. W.; and Meyers, J. F. (2005): *Increased Accuracy in Molecular Filter Based Flow Field Diagnostics Through Direct Frequency Calibration Using Optical Modulators*. 43rd AIAA Aerospace Sciences Meeting and Exhibit, Paper 2005-0033, Reno, NV, January 10-13, 2005.

Meyers, James F. (1992): *Doppler global velocimetry – the next generation?* AIAA 17th Aerospace Ground Testing Conference, Nashville, TN, paper no. AIAA-92-3897, July 6-8, 1992.

Meyers, J. F. (2005): *Doppler Global Velocimetry Measurements of Supersonic Flow Fields*. VKI LS 2005-01, Advanced Measuring Techniques for Supersonic Flows.

Nobes, D. S.; Ford, H. D.; and Tatam, R. P. (2002): *Three dimensional planar Doppler velocimetry using imaging fibre bundles*. 40th AIAA Aerospace Sciences Meeting & Exhibit, Paper 2002-0692, Reno, NV, January 14-17, 2002.

Shirinzadeh, B.; Hillard, M. E.; Exton, R. J. (1991) Condensation effects on Rayleigh scattering measurements in a supersonic wind tunnel. AIAA Journal, 0001-1452 vol. 29 no.2 (242-246)

Willert, C.; Stockhausen, G.; Klinner, J.; Beversdorff, M.; Quest, J.; Jansen, U.; and Raffel, M. (2003): *On the development of Doppler global velocimetry for cryogenic wind tunnels.* IEEE 10th International Congress on Instrumentation in Aerospace Simulation Facilities (ICIASF), Göttingen, Germany, August 25-29, 2003.